Molecular
Biosystems

Volume 1 | Number 1 | Jan 2013 | Pages 1–100

www.rsc.org/molecularbiosystems

THE BIOLOGY
OF PLAGUE

ROYAL SOCIETY
OF CHEMISTRY

ROYAL SOCIETY
OF CHEMISTRY

www.rsc.org/molecularbiosystems

# Journal Name

## ARTICLE

# Multi-scale modeling of cell survival and death mediated by p53 network: A Systems Pharmacology Framework

Yuan Wang[a], Zihu Guo[a], Xuetong Chen[a], Wenjuan Zhang[a], Aiping Lu[b] and Yonghua Wang[*a]

Abstract  The determination of cell fate is a key regulatory process for development of complex organisms that is controlled by distinct genes in mammalian cells. To interpret the decision process into a rigorous, analytical framework, we performed a multi-scale simulation of cell fate decision mediated by the p53 regulatory network in a systems pharmacology framework. The model treats fate determination as a gradual response to stress that delays the initiation of apoptosis to give the cell an opportunity to survive. The newly proposed two-factors model: DNA-p53 coupling explains the phenomenon of the existing biological responses to stress damage for p53 regulating network. In addition, the model also reveals the cell survival rate can be improved by lowering the p53 level in a feed-back network to increase its robustness for external stimuli. The present work not only deepens our understanding of cell fate determination, but also provides a theoretical basis for rational drug discovery and development.

## Introduction

In multicellular organisms, homeostasis is maintained through a balance between cell proliferation and cell death, which refers to the regulation of synthesis of molecules within the cell as well as the organization and function of cells and tissues.[1] Cell survival and death appear when the homeostasis is disrupted, and the dysregulation play important roles in the pathogenesis of many complex diseases. The determination of cell fate has been investigated with both an experiment and mathematic model simulation, and is regulated by both cell-intrinsic and cell-extrinsic factors. Although much is known about the lot number of proteins are shown a close relationship about the cell apoptosis, less is known about the mechanisms of cell death. So elucidation of the mechanisms of cell-fate determination and the search for chemopreventive agents are important and urgent tasks.

The p53 protein is a major protein in the elucidation of cell fate through two aspects: the single-cell and multiple-cell levels. The gene expression dynamics and the natural oscillators of p53-Mdm2 have been obtained in response to DAN damage caused by gamma irradiation and a series of discrete pluses in identical cells.[2, 3] However, the expression of other related-factors of p53 network (PTEN, p21, ARF, etc.) has not yet been shown, which are pivotal downstream targets of p53 regulatory network.

Recently, a series of mathematical models have been proposed to explain the dynamics and kinetic processes of p53 stress response network under certain treatment, either in cell population or in a single-cell, and most of which are deterministic model produced by ordinary differential equations (ODEs).[4-8] These mathematical models of the dynamics of p53 signalling pathways make it possible to understand the decision of cell survival or death through systems-based dynamic analysis. Unfortunately, the existing modelling efforts have not explored sustained pulses as found on internal and external stress responses, respectively, and also have not explained why the survival and death can be observed for the same samples treated by the same conditions.

In this study, we propose a multi-scale systems pharmacology-based framework to simulate the p53-dependent cellular stress response in single-cell and multiple cell levels for cell fate determination, respectively. The model is consisted of three modules: a DNA damage repair module, an ataxia telangiectasia mutated (ATM) switch, and the p53 network. The Cellular Potts Model (CPM) coupled with ODE is applied to investigate the stress response of p53 network in the cell-fate determination process. Based on the dynamic results, we attempt to establish a two-factors randomized mathematic model to explain the cell-fate determination. Our approaches and modelling results have provided valuable ideas to achieve the relationship between the monitoring of multidimensional (different conditions, times, and proteins) pathway dynamics and cell behaviour.

a. Lab of Systems Pharmacology, Center of Bioinformatics, College of Life Science, Northwest A&F University, Yangling, Shaanxi, 712100, China.
b. School of Chinese Medicine, Hong Kong Baptist University, Kowloon Tong, Hong Kong.

## Methods

**The model of p53 regulatory network**

Molecular BioSystems Accepted Manuscript

ARTICLE

Journal Name

The model involves two repair ways of double-strand DNA breaks (DSBs), ATM, two-compartment kinetics of p53, its primary inhibitor Mdm2, phosphatase PTEN, PIP3, Akt kinase, p21, Myc, Mucin1, cdk2/cyclin E, Siah-1, beta-catenin, p19/14ARF and miR-145. The transcriptional activity of p53 is regulated by a complex network that involves all the mentioned molecules (Fig. 1), and the details are as following:

1) In the cell nucleus, under the continuous effect of acute ionizing irradiation (IR), DSBs generate and trigger two major repair mechanisms: homologous recombination (HR) and non-homologous end joining (NHEJ) (denoted *DSBs*).[9] The DNA complex (DSBCs) formed by DSB and repair proteins Mre11, Rad50, and the repair process contains both the fast kinetics and the slow kinetics (denoted by *DSBCs1* and *DSBCs2*, respectively), resulting in the fixed DSBs (denoted by *Fixed DSB1* and *Fixed DSB2*, respectively).[5, 10] Meanwhile, about 60–80% of DSBs are rejoined quickly, whereas the remaining 20–40% of DSBs are rejoined more slowly.[5, 11]

2) DSBCs induces the activation of ATM, the rapid acetylation and intermolecular auto phosphorylation, causing the dimer to dissociate rapidly into the active monomers (denoted by *ATMd*, *ATM* and *ATMa*, respectively).[12, 13]

3) The p53 protein is phosphorylated by ATM, the unphosphorylated proteins further undergo reversible phosphorylation (with unphosphorylated and phosphorylated p53 denoted by *p53* and *p53a*, respectively), and degradation processes. At the same time, the activation of AKT is mediated through ATM in vivo.[14]

4) The p53 protein activates transcription of the murine double minute gene (denoted *DNA-Mdm2*), which transcripts (denoted by *mRNA-MDM2*), translates to Mdm2 protein. The unphosphorylated proteins further undergo reversible phosphorylation, and degradation processes. In the cytoplasm, the Mdm2 protein can target p53 for its degradation.[2]

5) The p53 protein induces the transcription of the *PTEN* gene (denoted *DNA-PTEN*), coding PTEN protein (denoted *PTEN*), which acts as a phosphatase for PIP3 protein, and the phosphorylated proteins further undergo reversible dephosphorylation (with unphosphorylated and phosphorylated PIP3 denoted by *PIP2* and *PIP3*, respectively), and degradation processes. The PIP3 protein regulates the phosphates of AKT protein, and the phosphorylated proteins further undergo reversible dephosphorylation (with unphosphorylated and phosphorylated AKT denoted by *Akt* and *Akta*, respectively), and degradation processes. The AKT protein mediates the phosphorylation of Mdm2 protein.[15-17]

6) The p21 protein (denoted *p21*), encoded by the *WAF1/CIP1* gene (denoted *WAF1/CIP1*), can be transcript-activated by p53 protein,[18] and undergoes degradation processes. Meanwhile, the transcription is mediates by ARF protein[19] and Myc protein.[20] p21 protein can bind to cdk2/cyclin E (with unphosphorylated and phosphorylated cdk2/cyclin E denoted by *Cyclin E/cdk2* and *Cyclin E/cdk2a*, respectively) and inhibits its function.[21]

7) The Siah-1 protein (denoted *Siah-1*), encoded by the *SIAH1* gene (denoted *SIAH1*), can be transcript-activated by p53 protein,[22] and undergoes degradation processes. At same time, it mediates beta-catenin protein (denoted *Beta-Catenin*) degradation,[23] as p53 protein.[24]

8) The p19/14ARF (denoted *P19/14ARF*), encoded by the *INK4a-ARF* gene (denoted *INK4a-ARF*), is mediated by p53 in the transcript process, and can interact directly with p53, in turn mediate the transcription of p21 and inhibits the Mdm2 ubiquitin ligase.[19, 25]

9) The model also incorporates the functions of miR-145, which can be transcriptionally induced by p53,[26] i.e., miR-145 inhibits the activation of AKT protein,[27] and plays the roles in the posttranscriptional regulation of c-Myc and Mucin1 proteins (denoted *mMyc* and *Myc*, *mMucin 1* and *Mucin 1*, respectively).[26, 28] At same time, c-Myc and Mucin1 also induce transcription of the ARF,[29, 30] and Mucin1 increases beta-catenin levels in the cytoplasm,[31] c-Myc can influence the outcome of p21.[20]

In summary, this model displays the regulatory network of p53 response on the damage of DNA, which is combined with positive and negative feedback loops, is co-activation of 11 proteins and miR-145. The detailed pathway is shown in Fig. 1.

The detailed network model incorporates Hill-type, Michaelis-Menten and mass action kinetic, which are the mathematical models that explain and predict the behaviours of molecules in governed by a system of kinetic Equations (S1)-(S36) (Supplementary Methods), and the parameter values are shown in Supplementary Table S2.

**Dynamic sensitivity analysis**

In this work, a dynamic sensitivity analysis is used to study the time-varying sensitivities in the biological systems and individual parameters are varied and the effects of such variation on the output of the system are evaluated.[32, 33] The steady-state concentration fluxes of reactions were defined as system output. In our model, the sensitivity coefficient is calculated as

$$S = \frac{\partial Y}{\partial X_i} \tag{1}$$

where S is the sensitivity index of the state variable Y (representing the model output) to the parameter $X_i$. The results are normalized to obtain the scaled sensitivity coefficients S' that is dimensionless.

**A two-factors model of cell fate determination**

In this section we attempt to propose a two-factors model to explain the existence of apoptosis rate, as a measure of cell-fate determination of the cell population.

In p53-related apoptosis experiments, the concentration of p53 protein and the cell damage level are both relative to apoptosis. So we use X(t) to express the possibility of apoptosis

*Journal Name* ARTICLE

induced by factors at time t, and set the level of X(t) is proportional to the number of p53 protein ([p53](t)) and the intact DSB numbers ([DSB](t)) (denoted by P and M, respectively), X as Eqs. (2)-(3) describe:

$$X \propto P \tag{2}$$

$$X \propto M \tag{3}$$

then we assume the relationship can be described as following:

$$X(t) = k \times P \times M \tag{4}$$

here,

$$P = [p53a](t) \tag{5}$$

$$M = [DSB](t) \tag{6}$$

therefore, substituting *P* and *M* into Eqs. (4), we obtain

$$X(t) = k \times [p53a](t) \times [DSB](t) \tag{7}$$

then, X(t) should carry out linear function conversion normalization, the equation is:

$$y = (x - \text{MinValue}) / (\text{MaxValue} - \text{MinValue}) \tag{8}$$

x is X(t), y is the normalized X(t), MaxValue is the maximum value, MinValue is the minimum value. The normalized X(t) are all in [0,1].

The cell mutation rate at time t is marked as R(t), so $\{R(t), \ t \geq 0\}$ is a stochastic process, where $R(t)=AX(t)$ and $A \sim U[0,1]$.

### The Glazier-Graner-Hogeweg or *GGH* Model

In order to validate the experimental data obtained in the study of single and multicellular for p53, we use mathematical approaches with the *GGH* model, also known as the CPM,[34, 35] which uses the spatially extended domains on a fixed lattice, usually 3D Cartesian lattice or 3D hexagonal lattice to represent cells, and the dynamics of cells is described by effective energy formalism and implemented as a Monte Carlo algorithm. For each pixel copy attempt, the change in the overall system effective energy $\triangle H$ and accept the attempted pixel reassignment with probability P(ΔH):

$$P(\Delta H) = \begin{cases} e^{\left(-\frac{\Delta H}{kT}\right)} & \Delta H > 0 \\ 1 & \Delta H < 0 \end{cases}$$

(10)

here Δ*H* shows the difference in effective energy produced by the change, k is a converting constant, and T represents a parameter corresponding to the amplitude of cell fluctuations.

The effective energy, also called the Hamiltonian and denoted by either H or E, is the core of the *GGH* model. The Hamiltonian is typically expressed as a sum of terms, each term representing different cellular behaviors, interactions, mechanics, etc. The effective energy mixes true energies such as cell-cell adhesion with terms that mimic energies. In our simulations we have used Hamiltonian containing contact

energy, and two terms implementing constraints on cell shapes (volume and surface).

$$H = \sum_{\tau_1 \tau_2} J_{\tau_1, \tau_2} (1 - \sigma_{\delta(i), \delta(j)}) + \gamma_s (S_1 - S_2)^2 + \gamma_v (V_1 - V_2)^2 \tag{11}$$

The first term describes the contact energy between cells, and their environment, i and j represent the cell ID, $J_{\tau_1 \tau_2}$ represents the adhesive energy per unit area between type $\tau_1$ and type $\tau_2$, $\gamma_s$ and $\gamma_v$ are related to surface and volume elasticity, respectively. σ expresses the Kromeke-σ-function, S1 and S2 denote the current surface and the target surface, $V_1$ and $V_2$ express the current volume and the target volume, respectively.

### Algorithm Implementation

To simulate apoptosis behavior related with p53 network inside individual cells vary over time, we write functions in our CC3D-Bionetsolver code to record values to output files of all concentrations each Monte Carlo Step (MCS), and perform the simulation by CompuCell3D (http://www.compucell3d.org)[36] on a domain or a lattices of 100×100×1 pixels in x, y, and z directions, respectively, with the z-axis being perpendicular to the page. All cells are individually created in the shape of a cube of size 10×10×1 pixels, without gaps between them and each cells were regulated by mentioned network. In the lattice, we place a sheet of cells with 10 cells along x-axis, 10 cells along the y-axis, and 1 cell along the z-axis. A scale of 1 pixel equal to 1 μm was used. Therefore one cell has a volume of about 100 μm$^3$. The initial configuration is one single cell surrounded by a number of similar cell. The cells in our model are nonpolar, with the exception of Source cells, and have a constant volume and do not divide or growth, and hence cell fate is driven by the p53 regulate network dynamics. The determination of cell fate is expressed only by the probability that a given cell will or will not change color.

To simulate the determination of cell fate we introduce two types cell (apoptotic cell and non-apoptotic cell). A cell type denotes a collection of model cells that share a unique set of properties, interactions and dynamics. The cell types result from cell state in which some genes turn on or activate and other genes turn off or inactivate. As a result, different cell types represent different behaviors. In the CPM, all cells of a particular differentiation type share a set of parameters describing their behaviors and properties. All CPM models use MCS as a unit of time, and each MCS consists of number of pixel copy attempts equal to total number of lattice sites. The conversion between pixel and physical distance (or MCS and physical time) depends on model parameters. In our simulations 1 MCS corresponds to 1 min of real time and the parameters in the multi-scale model are scaled accordingly.

## Results and discussion

### Dynamics of p53 network for internal stresses

Molecular BioSystems Accepted Manuscript

**ARTICLE**

The nonuniform distribution of dislocations in proteins and other organic and bioorganic molecules gives rise to internal stresses that determine cell response. The mechanical response of p53 regulatory network is essential for survival in a stressful intracellular environment. Different cells might face different internal stresses. Therefore, we focus on the dynamic behaviors of p53 regulatory network in cells with changeable internal stresses in this section.

The p53 network that we consider in this work is shown schematically in Fig. 1. We separately obtain its overall qualitative dynamic behavior by analyzing its bifurcation diagram, which is relatively independent of the model parameters (shown in Supplementary Table S2). In this network, ATMa can be as one representative of stress integrators. So the dynamic behaviors of p53 network under changeable internal stress can be simulated by the increased fixed levels of activated ATM protein, and the results are shown in Fig. 2.

Among the predictions of the model is that increasing levels of the fixed concentrations of ATMa or stress level drives the periodic change of the dynamic behavior of activated p53 protein: straight line, one pulse wave, damped oscillations, oscillation, damped oscillations, one pulse wave and logarithmic graph in stages, respectively (Fig. 2A). Ultimately, however, only two steady state forms: fixed and oscillation of concentration appear in all types of cell internal stresses. Interestingly, while the onset of oscillation requires a sufficient amount of ATM, an excessive total amount of ATM annihilates p53 oscillation, quite similar with the simulation results.[5]

At intermediate levels of internal stress cell, the concentration of activated p53 undergoes oscillation, while undergoes more pulses followed by basal levels in low-steady-state and high-steady-state. We postulate that in between two line-steady-state levels associated with low internal stress and high internal stress, there exists a range of activated p53 levels with oscillate state. We call this range the transforming zone. Furthermore, the concentration of p53a grows with the number of ATMa level or internal stress level in general, and the faster activated p53 grows, the higher internal stress level (Fig. 2B and C). This means the number of concentration of activated p53 is lower in lower-internal-stress normal cell than higher-internal-stress diseased or cancer cell.

Dynamic analysis of the p53 regulation shows a bifurcation diagram of activated p53 concentration as a function of stress level (Fig. 2C). With increasing stress level, the activated p53 protein undergoes transitions form low steady state to oscillation to high steady state. Oscillations appear at the intermediate levels of stress level, with a period about 250 min; a high steady state appears at higher stress level. These results are consistent with existing experimental observations and theoretical modeling.[2, 37, 38] Moreover, the first pulse is slightly higher than the second, quite similar as the experimental observations[2] and the simulation results.[5, 6]

The existence of the transforming zone increases with internal stress level, the cell always passes through the entire oscillation phases. Because there are molecular interactions among p53a and other molecules, here we consider a system with ATMa = 1.73 as a representative to illustrate this (Fig. 2D). The simulation shows that the regulatory system is robust in the transforming zone. Fig. 2D illustrates the traces of oscillations between p53a and Mdm2a with the same frequency and different swing (details of other molecules are shown in Supplementary Fig. S1). In the transforming zone (the equilibrium state), the system undergoes oscillations with less frequency along with the increasing internal stress levels (Fig. 2E). It is shown that p53a and Mdm2a responses by cyclic behavior way in individual cells (Fig. 2F), which is supported by previous work.[2] This illustrates the significant concentration differences between p53a and Mdm2a to keep robustness against the internal stress.

Dynamic analysis of the p53 regulation module reveals the dynamic behavior of p53a protein undergoes transitions from low steady state to oscillation, and to a higher steady state, with increasing cell stress levels. Oscillations appear at the intermediate levels of cell stress. A high steady state appears at higher cell stress level. These results are consistent with experimental observations and theoretical modeling.[5, 37] Fig. 6B demonstrates the extraordinary regularity and long-term stability of the oscillations at ATMa = 1, 1.73 and 2.5. When ATMa is increased, p53a is increased, and the limit cycles, formed by p53a and its major negative factor-Mdm2a, are shown in Fig. 6C. The result shows the higher ATMa levels, the lager distribution of cyclic fitness.

**Dynamics of p53 network for external stress**

Here, we illustrate how these systems responds to different levels of external stress. That is, we find three subjects, two in the treated groups (short-time one and continuous one) and one in the control group. Through the first 2000 min simulation, each system is at steady states as shown in Fig. 2 (see the gray area in Fig. 3). Upon external stress, a different number of pulses response to short-time group, while the oscillation and logistic-like up-regulation response for p53 network to continuous external stress.

For short-time group, IR = 5 Gy for 20 min, as a representative, the levels of p53a are sharply increase immediately, and then undergo certain pulses followed by their original levels after removing IR (see the red dash-dot lines in Fig. 3). For the internal stress lower than the transforming zone system, the higher intrinsic stress, the more pulses undergo and longer time used to return their original levels for same external stress (Fig. 3A to C). For the higher system, only one concentration pluses of p53a is used to response the short-time treatment, and return the originals levels at 3000 min almost after remove IR (Fig. 3E to G). Meanwhile, in the transforming zone, the period of oscillation is delayed, with same frequency and amplitude after tiny up-regulation some time (Fig. 3D).

These simulations suggest that, for short-time external stress, the robustness leads to return the original cells' states,

**Journal Name**

**ARTICLE**

ultimately. On the lower internal stress system, the higher internal stress would make the robustness weaken, and displaying the weakening ability to adapt to changed circumstances. While facing higher stress, the system loses the ability to fit for changes on damped oscillatory response, which is the major response form for lower system. During the range of transforming zone, the period of cell is delayed but the state of cell is no change.

To obtain deep insights into the mechanisms of different responses for all kinds of cells under continuous external stress, we consider the DNA damage level in the system with 5 Gy to simulate, where it is used in experiment to study how p53 performs its function as a nuclear transcription factor, regulating the expression of target gene in response to DNA damage.[39, 40] The results are shown in Fig. 3 with green dash-dot lines. Notably, there are three kinds of response for seven levels system under continuous 5 Gy treatment, such as oscillation, damped oscillation and logistic-like up-regulation, with the increased internal stress system. This means the network responses to external stress in an oscillation way in the lower internal system while a damped oscillation way in the transforming zone system, but losing its robustness on higher internal stress.

It is noteworthy that two kinds of steady state levels are observed similarly with the internal stress: stationary level and oscillation level. Compared with control group, the fluctuating form is the major way to response external stress. This can explain why p53 is oncogen and tumor suppressor gene, as p53 induces growth arrest through control on a lower level in cell, while initiates apoptosis on a higher level due to loss of robustness for the system.

It is noteworthy that these results are anastomotic with experiment results:[2] 1) Different cells from the same clone in the same field of view showed different numbers of oscillations, with cells showing either zero, one or two pulses (some cells began a third pulse towards the end of the movies). The low steady state simulation results get this result similar (Fig. 3E G F and D). 2) The width of each pulse in our model are almost 300 min accorded with the experimental area 350 ± 160 min (mean ± s.d.). 3) Pulse heights varied by approximately threefold between cells (see the blue and magenta line in Fig. 1A).

The simulation shows that more highly robust ability in lower stress level system, while lost the ability in high steady state system. These provide an evidence-based window to explain the seemingly contrary mechanisms of p53 protein: arrest growth by holding the cell cycle at the G1/S regulation point on DNA damage recognition (if it holds the cell here for long enough, the DNA repair proteins will have time to fix the damage and the cell will be allowed to continue the cell cycle), and initiate apoptosis-programmed cell death - if DNA damage proves to be irreparable. Hence, we have successfully put forward a model, which can predict the p53-related network behavior under a constant confinement pressure.

### Dynamic sensitivity analysis of p53 networks

In order to understand the dynamic properties of the system with changes in parameters, and found which parameters are more important in the system. We performed a sensitivity analysis and the results are shown in Supplementary Fig. S2. A positive value of S (scaled sensitivity values) indicates an increase, and a negative value indicates a decrease in the system output upon the changes of the respective parameter. The scaled sensitivity absolute value $|S|>1$ suggests that changes in reaction rate may have an amplified effect on the reaction output. Here a total of 12510 (139 parameters×90 reactions) local sensitivities for the network were calculated and obtained 82 $|S|$ values for 47 parameters and 23 reactions >1 (Fig. 4).

It is found Jcf has the largest impact on the whole pathway, affecting 5 out of a total of 23 reactions with $|S|> 1$ and 11 out of all reactions with $|S|> 0.75$. About the most important element p53, 39 $|S|$ >1, for 28 parameters and 8 reactions. Another major element Mdm2 also shows 19 $|S|$ for 19 parameters and 6 reactions >1. These observations explain why the two core proteins Mdm2 and p53 very important in the whole network. Meanwhile, the reactions miR-145 formation by p53a shows 8 $|S|$>1, for kfg, kcf, Jcf, δf, kah, ni, σi, kct and Jct, which are the paraments for the mRNA-Mdm2 translation reaction, the mRNA-Mdm2 translation by p53a reaction, the mMdm2 degradation reaction, the Mdm2a degradation by ATMa reaction, etc. these results shows the element miR-145 can be regualted by p53, and feed-back regulat p53 through element Mdm2.

### Kinetic parameter effects

Here, in order to further investigate the dynamic effects of kinetic parameters between two core protein p53a and Mdm2a, the rate constant ($J_{cf}$) was increased or decreased by 20% compared with the 'basal' value of $J_{cf}$ =1, shown in Fig. 5A and B. The oscillations show with the same frequencies for mMdm2, Mdm2a and p53a, indicating the robustness of the network. Once $J_{cf}$ is downregulated by 20%, mMdm2 is also down-regulated but an up-regulation of Mdm2a appeared simultaneously.

In addition, we have also tested the sensitivity of the incomplete network without the p21 (Fig. S3). We found only 76 $|S|$ values for 23 reactions >1. Comparing to the results of Fig.4, only 9 scaled $|S|$ values for 10 parameters ($J_{cf}$, $k_{ad}$, $δ_f$, $σ_d$, $k_{eg}$, $k_{ed}$, $k_{wu}$, $δ_i$, $σ_j$ and $k_{jk}$ have changed, with 6 scaled $|S|$ values significantly up-regulated, and 3 scaled $|S|$ significantly down-regulated, but others remains unchanged. The ckd2a degradation reaction is the most obvious down-regulated reaction and the Mdm2 phosphorylation by cdk2a is the second one, that shows the p21 regulate the netword mainly through cdk2a and Mdm2.

### Cell fate determination by two factors: p53 and DNA damage

**ARTICLE**

Exposure to cellular stress can trigger the p53 tumor suppressor to induce cell growth arrest or apoptosis. In response to DNA damage, p53 can be a strong inducer of apoptosis. This function is dependent on the cell type as well as type and extent of the DNA damaging agent. The intracellular activated p53 level has been shown to exhibit a series of pulses after DNA damage caused by ionizing radiation.[41, 42] So, Zhang et al. demonstrate that cell fate is determined by the number of p53 pulses relying on the extent of DNA damage. That means the cell fate has relationship with DNA damage, and the extent of external stress can change the cell fate through p53 network.

What is noteworthy is that the active p53 protein in 1.73 system (green line in Fig. 3D) changes the oscillation behavior to damped oscillation under short-term treatment, like the dynamic waves in 3.47 system without treatment group (blue line in Fig. 3E). That says only p53 protein level cannot determine cell fate in earlier model calculations. Therefore, we constructed a two-factors model to reveal the relationship among p53 protein, cell damage and cell fate (see more details in Method section).

The existence of apoptosis rate in the molecular biological functional studies means partial cell still remain their original states even after certain treatment. That is, the responses of p53 regulate network for identical external stress are different, some are survival, while others apoptosis. Our two-factors model show a reasonable way to explaining these phenomenon.

Based on the simulation of p53 regulatory network, the representation of results, evaluated according to equation (1)-(9), show the dynamic behavior of apoptosis rate - Xt in seven systems (Fig. 6).

For short-term stimulation, the level of Xt quickly rises to its maximum and down-regulates after remove the treatment, eventually arrive at zero, and then finish the response of the damage (left of Fig. 6A). The normalized results show the same trend (left of Fig. 6B). More normalized results for short-term stimulation are shown in Fig. 64 (A, C and E). These results indicate cell occur apoptosis easier at early state after removing the damage treatment.

However, the level of Xt in continuous stimulation simulation rise in the oscillation way in low steady state system and oscillation system (see the red, green, blue and magenta line on right of Fig. 6A), while on the logistic-like up-regulation way in high steady state system (see the cyan, dark-green and brown line on right of Fig. 6A). The normalized results show the same trend (right of Fig. 6B), with short-term stimulation in Fig. S4 (B, D and F). It is demonstrated that cell apoptosis rate has oscillation-like behavior in low steady state system and oscillation system, while losing the ability of oscillation-like regulation under this treatment.

**Multi-scale modeling of the two factors model**

In this section, we study the growth and evolution of cell mass that consists of the apoptosis response of normal cells with varying spatial protein level and damage degree in order to understand the apoptosis effect and mechanism, using mathematical approaches with the GGH model coupled with ODEs (see more details in Method section), and the results are shown in Fig. 7.

All the simulation begin with 100 normal cell at the center of the domain. This initial cell divides repeatedly following the ODEs governing the dynamic behavior and eventually induces cell apoptosis. Following the CPM methodology we measure time in units of MCS. In our model a single MCS corresponds to 1 min of real time. At each MCS, all the cells are checked for the apoptosis rate levels and their phases are updated. Calculated Xt, the apoptosis marked by blue colorcell, while the un-apoptosis cell showed by green color. Fig. 7 shows the spatial distribution of the cells and Xt level at two different groups time points to show the cell fate under two kinds treatments.

For short-term stimulation (5 Gy 20 min) (Fig. 7A), about 13 percentage cell apoptosis, and almost 90 percentage occurs in the first 10 MCS (the raw data show on Table S3). Fig. 7C shows the number of apoptosis cell at various time points. Based on results of twenty times simulations, the two-factors model is proved steady. This means a positive correlation between the number of apoptosis cell and the level of Xt. The continuous stimulation (Fig. 7B) shows that almost 90% cell apoptosis appears at 32 MCS. That is say that the vast majority of cell are death under continuous stimulation for half an hour (for example, IR). It provides direct evidence of the necessariness of longer than 30 min in ultraviolet disinfection.

We also select an oscillation system (ATMa = 1.73) to simulate the two groups (Fig. S5). Compared with the two systems, the more the apoptosis cell, the higher internal stress, under same simulations (Fig. 8). It is suggested that it is easier to induce cell death on higher cell stress, which is consistent with experiment: at the higher dose of 7.5 Gy, the surviving fraction was low in both T47D/BP-3 and T47D/VEC.[43]

For normal cells, it is important to keep robust response for stresses. This ability can effectively decrease the change of protein level in cellular signal response, and finally increase chances for survival. Fig. 9 show the simulation results between the normal network and the incomplete network, where the feed-back loop regulation of the core protein p53 by Mdm2a is blocked (the parameter khb and khc are changed to zero). When losing the ability of robust response, the level of p53 protein can be double or three times higher (at the left of Fig. 9A), the level of Xt raised two times for short-term stimulation and nine times for continuous stimulation, respectively. The apoptosis rate shows an obvious increase from 13±2.6% to 77.8±3.8% in short-term simulation. However, in a continuous stimulation, the apoptosis time is definitely decreased as shown in Fig. S6a and b. These results indicate that a network-regulation might offer an available way to return the disordered cell to a normal state.

*Journal Name*

ARTICLE

## Conclusions

To deeply inspect the mechanism of cell fate determination, we show a muti-scale mathematical model of p53 regulatory network. The major goal is to investigate the dynamics of protein signaling pathways and cell stress response process. The model is composed of four main sub-network: 1) a cell stress damage repair module; 2) a signal transduction ATM switch; 3) the p53 regulatory network; 4) a cell-fate determination model for apoptosis. We predict three main states: the low steady state, oscillation and high steady state of the signal response for the p53 network. We also propose a two-factors model to explain the decision of cell survival and death. The simulations also suggest that the robust response of the p53 network to response the internal or external cell stress. This work not only deepens our understanding of cell fate determination, but also provides a theoretical basis for rational drug discovery and development.

## Acknowledgements

## Conflict of interest

The author declares that he has no conflict of interest.

## Notes and references

1.  M. Thiriet, in *Control of Cell Fate in the Circulatory and Ventilatory Systems*, Springer, 2012, pp. 279-327.

2.  G. Lahav, N. Rosenfeld, A. Sigal, N. Geva-Zatorsky, A. Levine, M. Elowitz and U. Alon, *Nature Genetics*, 2004, 36, 147-150.

3.  N. Geva-Zatorsky, N. Rosenfeld, S. Itzkovitz, R. Milo, A. Sigal, E. Dekel, T. Yarnitzky, Y. Liron, P. Polak and G. Lahav, *Molecular systems biology*, 2006, 2.

4.  A. Ciliberto, B. Novak and J. Tyson, *Cell Cycle*, 2005, 4, 488-493.

5.  L. Ma, J. Wagner, J. Rice, W. Hu, A. Levine and G. Stolovitzky, *Proceedings of the National Academy of Sciences*, 2005, 102, 14266.

6.  J. Qi, S. Shao, D. Li and G. Zhou, *Amino acids*, 2007, 33, 75-83.

7.  B. D. Aguda, Y. Kim, M. G. Piper-Hunter, A. Friedman and C. B. Marsh, *Proceedings of the National Academy of Sciences*, 2008, 105, 19678.

8.  K. Puszynski, B. Hat and T. Lipniacki, *Journal of theoretical biology*, 2008, 254, 452-465.

9.  J. Qi, Y. Ding and S. Shao, *Progress in Natural Science*, 2009, 19, 1349-1356.

10. R. D. Stewart, *Radiation Research*, 2001, 156, 365-378.

11. J. Budman and G. Chu, *The EMBO journal*, 2005, 24, 849-860.

12. T. Stiff, S. A. Walker, K. Cerosaletti, A. A. Goodarzi, E. Petermann, P. Concannon, M. O'Driscoll and P. A. Jeggo, *The EMBO journal*, 2006, 25, 5775-5782.

13. A. Dupré, L. Boyer-Chatenet and J. Gautier, *Nature structural & molecular biology*, 2006, 13, 451-457.

14. J. Viniegra, N. Martínez, P. Modirassari, J. Losa, C. Cobo, V. Lobo, C. Luquero, L. Álvarez-Vallina, S. Ramón y Cajal and J. Rojas, *Journal of Biological Chemistry*, 2005, 280, 4029.

15. T. Gottlieb, J. MARTINEZ LEAL, R. Seger, Y. Taya and M. Oren, *Oncogene*, 2002, 21, 1299-1303.

16. L. D. Mayo and D. B. Donner, *Trends in biochemical sciences*, 2002, 27, 462-467.

17. C. Blanco-Aparicio, O. Renner, J. F. Leal and A. Carnero, *Carcinogenesis*, 2007, 28, 1379-1386.

18. M. McVean, H. Xiao, K. Isobe and J. Pelling, *Carcinogenesis*, 2000, 21, 633.

19. T. Kamijo, J. Weber, G. Zambetti, F. Zindy, M. Roussel and C. Sherr, *Proceedings of the National Academy of Sciences of the United States of America*, 1998, 95, 8292.

20. J. Seoane and J. Hong-Van Le, *Nature*, 2002, 419, 729-734.

21. I. Shmulevich, E. Dougherty, S. Kim and W. Zhang, *Bioinformatics*, 2002, 18, 261.

22. G. Fiucci, S. Beaucourt, D. Duflaut, A. Lespagnol, P. Stumptner-Cuvelette, A. Géant, G. Buchwalter, M. Tuynder, L. Susini and J.-M. Lassalle, *Proceedings of the National Academy of Sciences of the United States of America*, 2004, 101, 3510-3515.

23. A. Iwai, H. Marusawa, S. Matsuzawa, T. Fukushima, M. Hijikata, J. Reed, K. Shimotohno and T. Chiba, *Oncogene*, 2004, 23, 7593-7600.

24. M. Oren, *Cell Death & Differentiation*, 2003, 10, 431-442.

25. R. Honda and H. Yasuda, *The EMBO Journal*, 1999, 18, 22-27.

26. M. Sachdeva, S. Zhu, F. Wu, H. Wu, V. Walia, S. Kumar, R. Elble, K. Watabe and Y. Mo, *Proceedings of the National Academy of Sciences*, 2009, 106, 3207.

27. M. Zhong, X. Ma, C. Sun and L. Chen, *Chemico-biological interactions*, 2010.

28. M. Sachdeva and Y. Mo, *Cancer research*, 2010, 70, 378.

29. D. Raina, R. Ahmad, D. Chen, S. Kumar, S. Kharbanda and D. Kufe, *Cancer Biol Ther*, 2008, 7, 1959-1967.

30. S. Adhikary and M. Eilers, *Nature Reviews Molecular Cell Biology*, 2005, 6, 635-645.

31. L. Huang, D. Chen, D. Liu, L. Yin, S. Kharbanda and D. Kufe, *Cancer research*, 2005, 65, 10413.

32. W. Wu, F. Wang and M. Chang, *BMC bioinformatics*, 2008, 9, S17.

33. X. Wang, Y. Li, X. Xu and Y. Wang, *Biosystems*, 2009.

34. J. A. Glazier and F. Graner, *Physical Review E*, 1993, 47, 2128.

35. F. Graner and J. A. Glazier, *Physical review letters*, 1992, 69, 2013.

36. M. H. Swat, G. L. Thomas, J. M. Belmonte, A. Shirinifard, D. Hmeljak and J. A. Glazier, *Methods in cell biology*, 2012, 110, 325.

37. Z. Li, M. Ni, J. Li, Y. Zhang, Q. Ouyang and C. Tang, *Journal of theoretical biology*, 2011, 271, 205-211.

38. X. P. Zhang, F. Liu and W. Wang, *Proceedings of the National Academy of Sciences*, 2011, 108, 8990.

39. M. K. Lee, W. W. Teoh, B. H. Phang, W. M. Tong, Z. Q. Wang and K. Sabapathy, *Cancer cell*, 2012, 22, 751-764.

40. G. Lahav, in *Cellular Oscillatory Mechanisms*, Springer, 2009, pp. 28-38.

41. X.-P. Zhang, F. Liu, Z. Cheng and W. Wang, *Proceedings of the National Academy of Sciences*, 2009, 106, 12245-12250.

42. G. L. Bond, W. Hu, E. E. Bond, H. Robins, S. G. Lutzker, N. C. Arva, J. Bargonetti, F. Bartel, H. Taubert and P. Wuerl, *Cell*, 2004, 119, 591-602.

43. A. J. Butt, S. M. Firth, M. A. King and R. C. Baxter, *Journal of Biological Chemistry*, 2000, 275, 39174-39181.
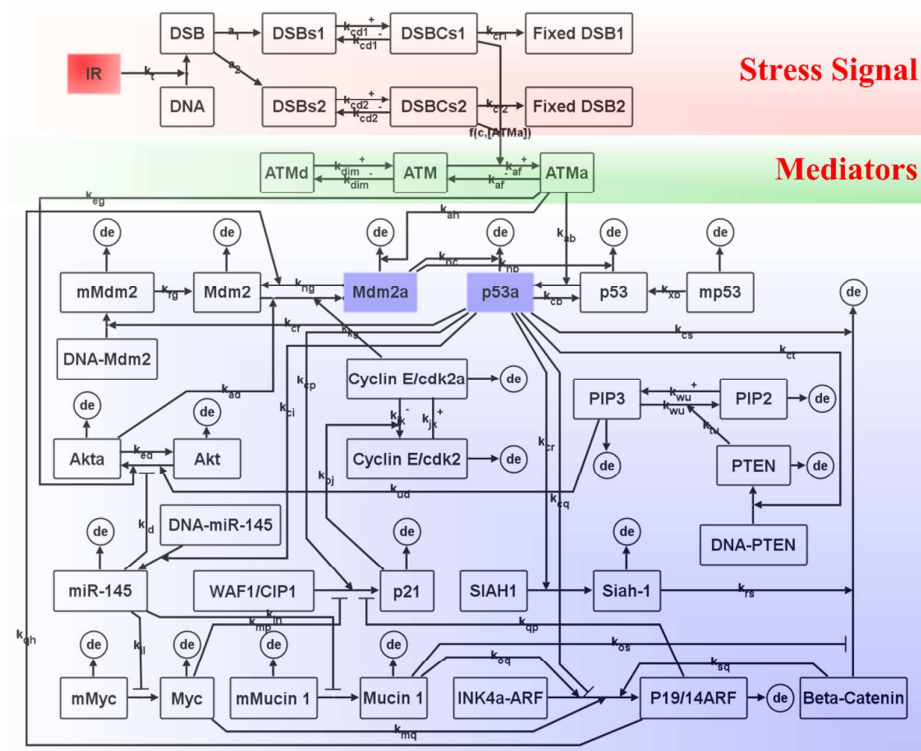
**Fig. 1** **The model of p53 regulatory network**

In this model, a rectangle represents a state for the concentration of mRNA, DNA or protein of one element, and the name suffixed by "a" represents the active form for the state of one element. The arrow represents the rate of different biochemical reaction, such as transcription, translation, phosphorylation, dephosphorylation or degradation. The arrow or hammerhead, which connects two tectangles of different elements, represents the rate of activate or inhibit reaction between two elements. The circle with "de" represents the degradation of one element. Abbreviations used: mMdm2, mRNA of Mdm2; mp53, mRNA of p53; mMyc, mRNA of Myc; mMucin1, Mucin1.
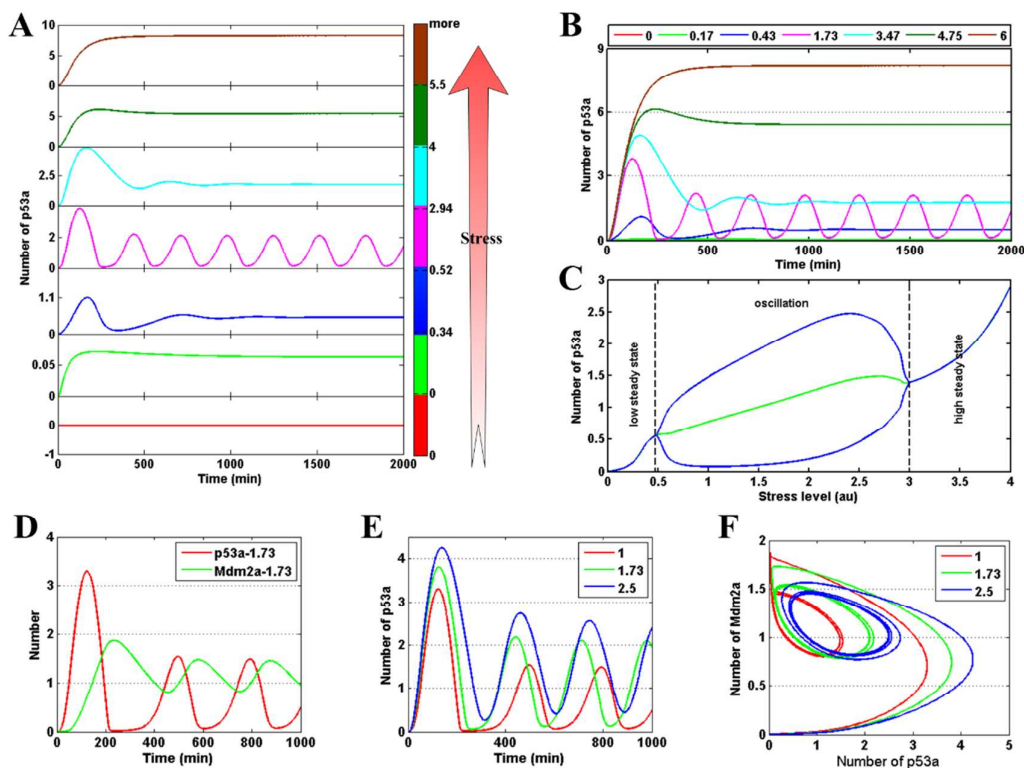
**Fig. 2 The dynamic behavior of p53 protein in systems**

(A) The kinetics of activated p53 protein under the increased stress levels. In special range of ATMa level, activated p53 protein shows the similarity dynamic behavior. (B) The kinetics of activated p53 protein under the middle level of each stress range. (C) The phase diagram of the activated p53 as a function of the DNA damage level (blue line). In the central region where activated p53 oscillates, the upper and lower branches denote the peak and valley values of the oscillation, respectively. (D) The time courses of the activated p53 (red) and activated Mdm2 (green) in transforming zone (ATMa = 1.73). (E) The time courses of the activated p53 at different levels in transforming zone (ATMa = 1, red; 1.73, green and 2.5, blue). (F) The relationship between the time courses of the activated p53 and the activated Mdm2 at same three levels with B.
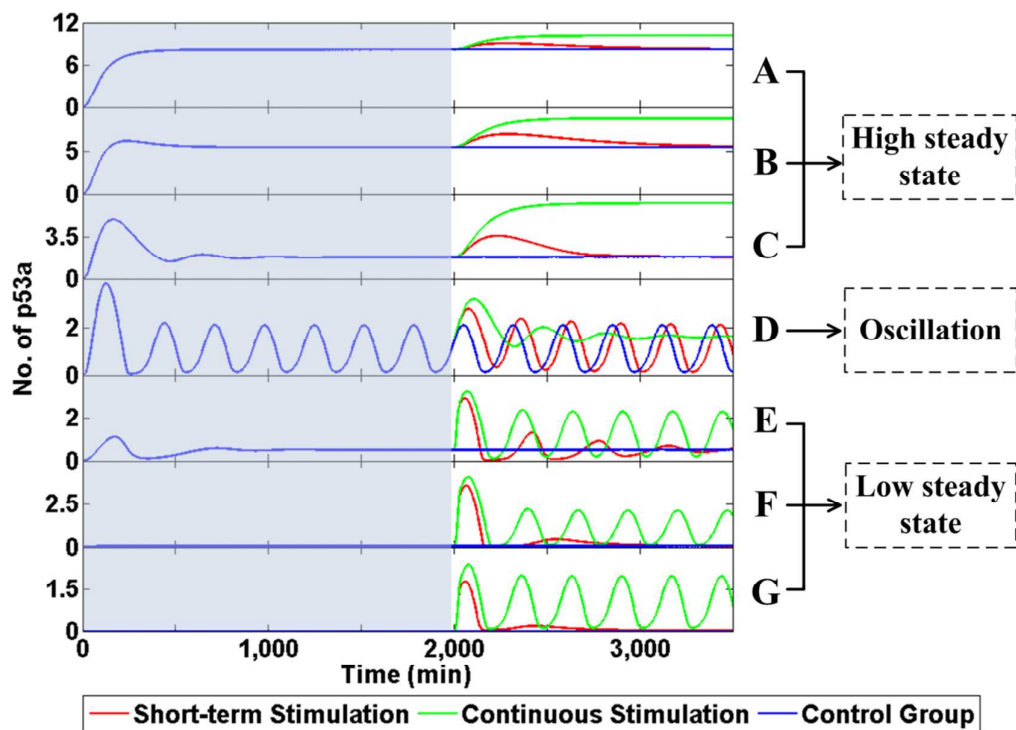
**Fig. 3 Whole-model simulation results**

After the first 2000 min simulation, the system is at steady state. Between time 2000 min and 4000 min, the control system undergoes changeable extrinsic stress. The red and the green dash-dot line represent short-time and continuous extrinsic stress, respectively, which is represented by 5 Gy IR for 20 min and continuous 5 Gy IR. The blue dash-dot line is the control group without any extrinsic stress. (A) to (G) represent the responses of the seven mentioned internal stresses cell under above three kinds treatments, represented by the value of ATMa is 0, 0.17, 0.43, 1.73, 3.47, 4.75, 6, respectively.
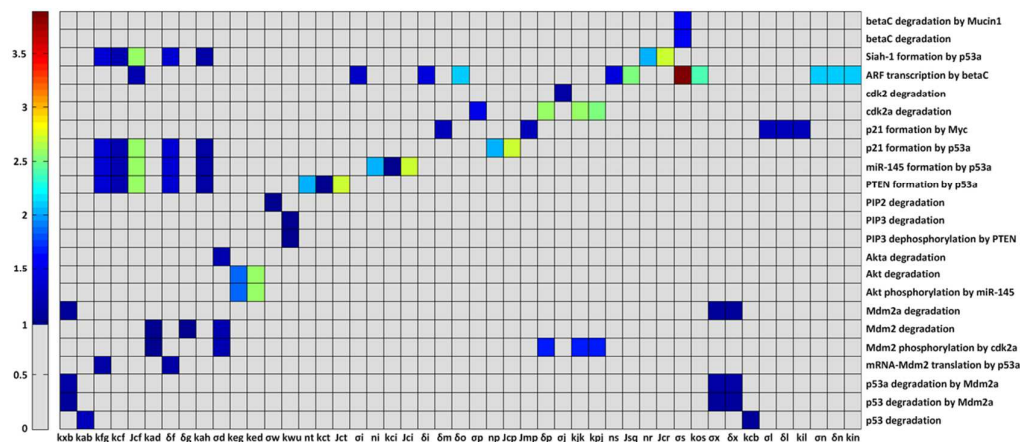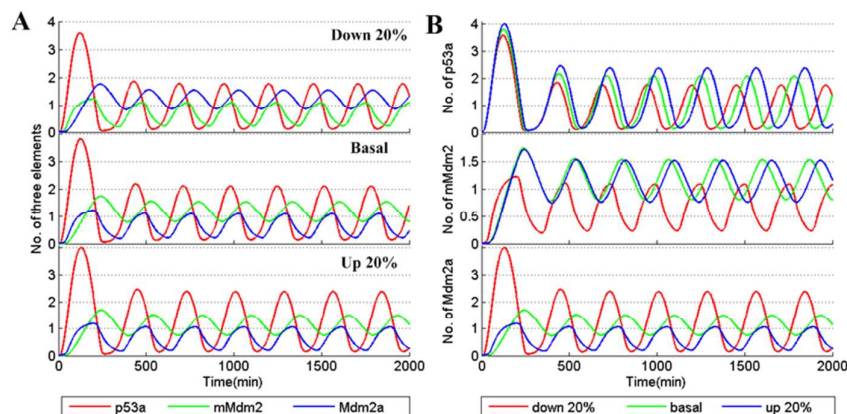
**Fig. 4 The heat map of 82 scaled |S| values for 47 parameters with 23 reactions >1.**

X axis represents a parameter with Y axis for a reaction flux.



**Fig. 5 Impact of the $J_{cf}$ on mMdm2, Mdm2a and p53a dynamics in the whole network.**

(A) p53a, mMdm2 and Mdm2a change with different Jcf values, by down 20%, bacal and up 20%, respectively. (B) The simulations of p53a, mMdm2 and Mdm2a are performed by three Jcf values of 0.8, 1 and 1.2.
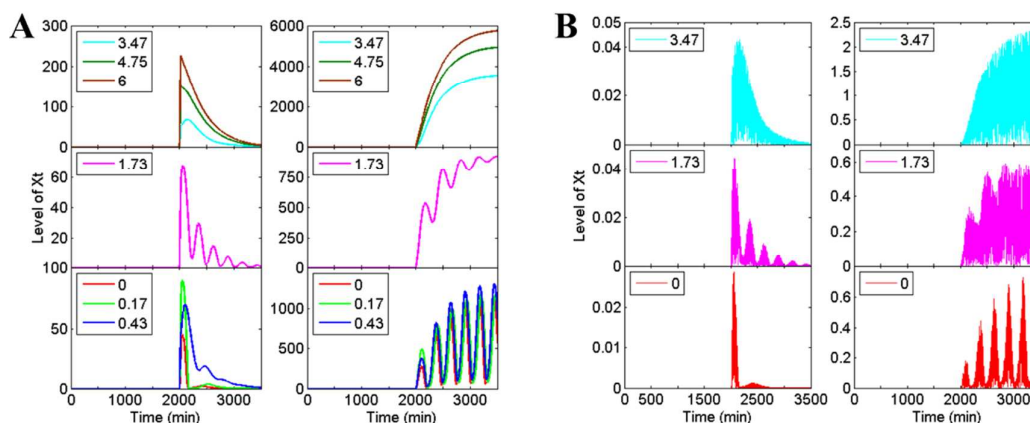


**Fig. 6 The dynamics of apoptosis rate-Xt in the above mentioned systems.**

(A) The level of Xt in seven systems under short-term (left) and continuous stimulation (right) are represented by red, green, blue, magenta, cyan, dark-green and brown line, respectively. (B) Red, magenta and cyan lines signify the normalized Xt in low steady state, oscillation and high steady state with two treatments (left: short-term stimulation and right: continuous stimulation), here, the MinValue is 0 and MaxValue is 1500.
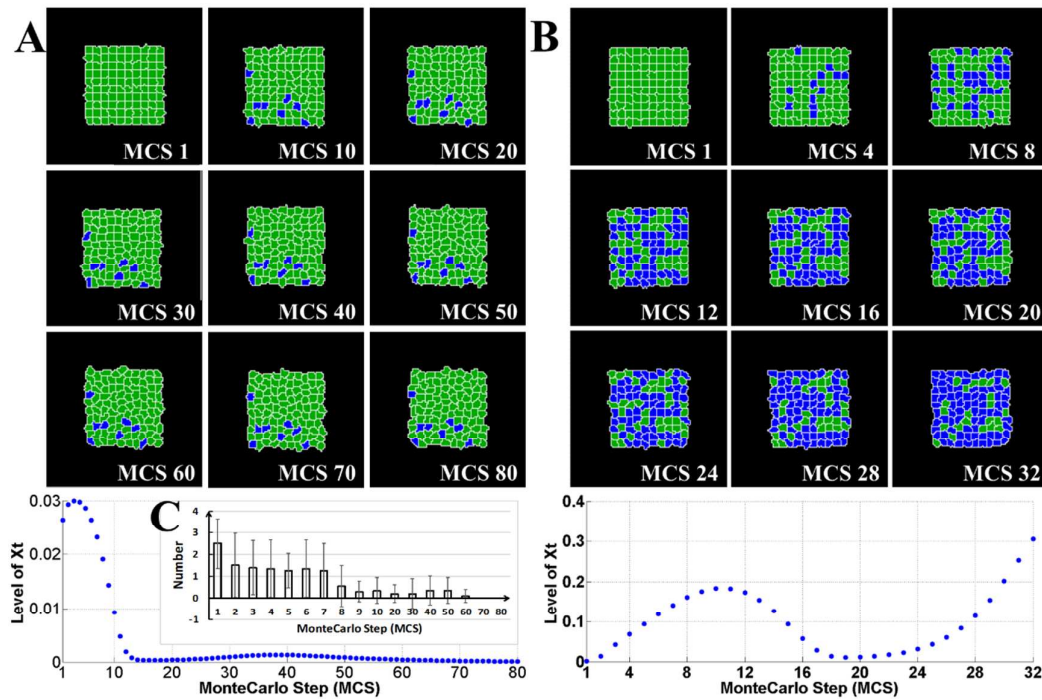
**Fig. 7 Plots showing snapshots of a sequence of the computation simulation results of the model at various time points.**

(A) and (B) denote the plots of the spatial evolution of cell fate in low steady state (e.g., 0 system) under short-term and continuous stimulation, respectively. Colours of the cells correspond to state of cell, green and blue represent cell survival and apoptosis, respectively. Plots of Xt levels for the simulation in which cells undergo special treatments. (C) The computation simulation results the number of apoptosis cell at various time points after short-term stimulation in aforementioned one of the low steady state 0 system. All simulations were performed twenty times.
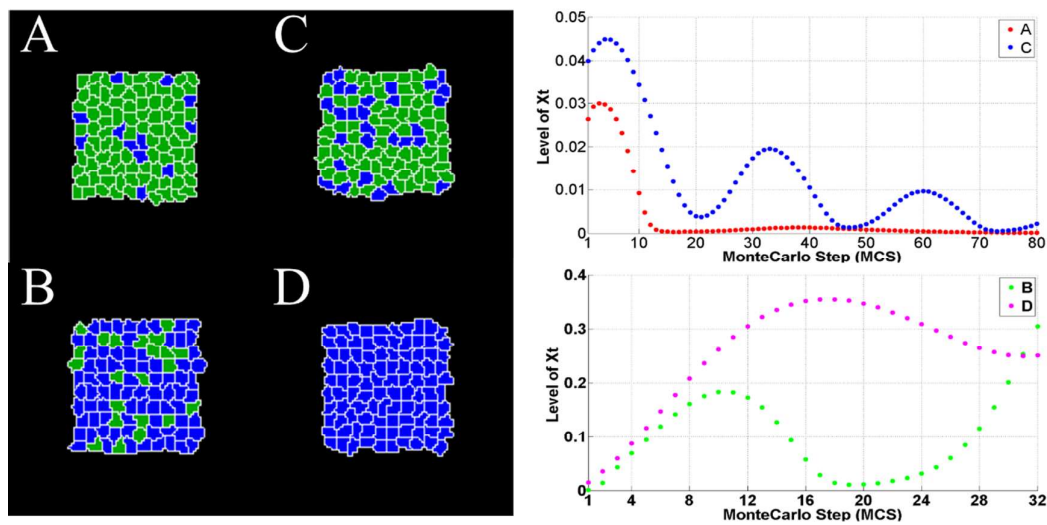
**Fig. 8 Plots showing the results of a simulation of cell fate determine.**

(A) and (C) denote in low steady state (e.g., 0 system) and oscillation state undergo short-term stimulation, while (B) and (D) undergo continuous stimulation. Plots of Xt levels for the simulation in which cells undergo special treatments.
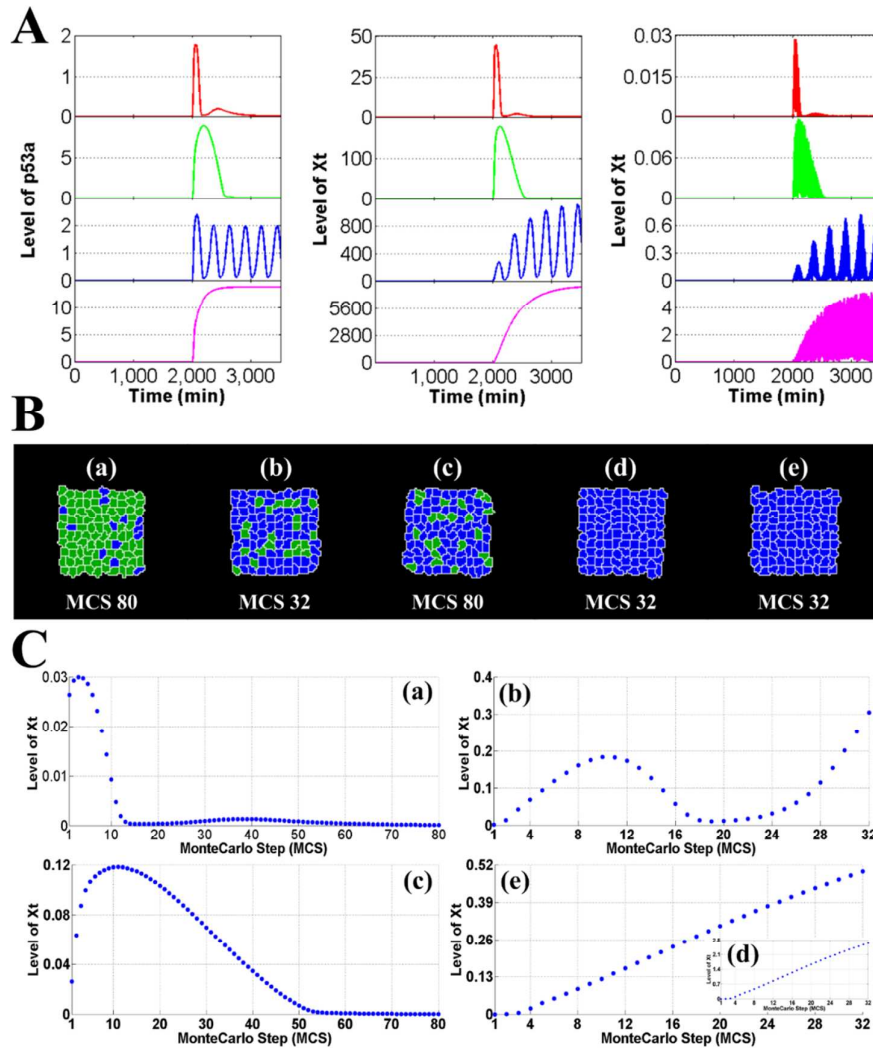
**Fig. 9 Plots showing the results of a simulation of cell fate determine.**

(A) the dynamic curves of p53 protein and Xt The red and blue line represents the normal system in short-term and continuous simulate, respectively, and the green and magenta line represents the incompletely system, respectively. (B) the snapshots of a sequence of the computation simulation results of two kinds system at special time points, (a) and (c) are the results of short-term group in two systems, and (b), (d) and (e) are the results of continuous group. Here the MaxValue is 1500 and 8000 in (d) and (e), respectively.